Cite this paper as: *Dalton Transactions*, 2019, **48**, 15036 - 15048, DOI: 10.1039/c9dt02876e

Computational assessment on the Tolman cone angles for P-ligands

Jesús Jover* and Jordi Cirera*

Departament de Química Inorgànica i Orgànica and Institut de Recerca de Química Teòrica i Computacional, Universitat de Barcelona,
Diagonal 645, 08028 Barcelona, Spain
email: jesus.jover@qi.ub.es, jordi.cirera@qi.ub.es

Abstract

The Tolman cone angle (θ), the par excellence descriptor of the steric measure of a phosphine, has been recomputed for a set of 119 P-ligands, including simple phosphanes and phosphites, as well as bulky biaryl species often employed in catalytic processes. The computed cone angles are obtained from three different transition metal coordination environments: linear [AuCl(P)] (θ_L), tetrahedral [$Ni(CO)_3(P)$] (θ_T) and octahedral [$IrCl_3(CO)_2(P)$] (θ_O), allowing to observe the steric behavior of the ligand when increasing the steric hindrance around the metal center. The computed cone angles have been extracted from the lowest-energy conformer geometry obtained with a combined MM/DFT methodology. A conformational screening is done using MM, which allows us to identify the lowest energy structure of each ligand in each coordination environment. These low energy conformers are subsequently reoptimized at DFT theory level, from which the cone angle value can be extracted. The computed cone angles are compared with the original Tolman cone angles, and with other steric parameters such as solid angles (Θ), percent buried volumes ($\%V_{bur}$), and angular symmetric deformation coordinate (S4'). This new set of values correlates with the phosphine ligand dissociation enthalpies in titanocene complexes of general formula [$Ti(2,4\text{-}C_7H_{11})_2(PR_3)$], and with reaction barriers in the Suzuki-Miyaura reaction

between [Pd-PR_3] and bromobenzene, proving that this newly proposed set of cone angles can be employed to establish linear correlations between different experimental and calculated properties for systems in which the phosphine ligands play a significant role.

Keywords: Phosphines, Tolman Cone Angle, DFT Calculations, Conformational Analysis

1. Introduction

Phosphines (PR_3) are among the most important and widely employed ligands in coordination chemistry. Known since 1870,[1] these compounds have some advantages over ammine ligands, such as their enhanced solubility in organic solvents and their compatibility with metals in multiple oxidation states. These two features have made metal-phosphine complexes very useful in the homogenous catalysis field.[2] Important chemical processes, including olefin hydrogenation (Wilkinson's catalyst),[3] olefin metathesis (Grubbs' catalyst),[4] or a wide range of palladium-catalyzed coupling reactions use metal-phosphine complexes.[5] Also, the tetrahedral nature of an sp^3 phosphorus atom with different substituents leads to a P-stereogenic center, and several transition metal complexes bearing such ligands have been used in enantioselective catalytic reactions.[6] It is precisely this high degree of functionalization, which allows controlling both electronic and steric properties of the phosphine ligand, what makes them highly effective in several chemical reactions. One of the first approaches to quantify the steric properties of the phosphines was done by Chadwick A. Tolman, when he proposed the Tolman cone angle (θ) as a measure of the steric bulk of the phoshphine ligand.[7] The Tolman cone angle is one of the most employed parameter for measuring

the size of a phosphine ligand. This parameter is defined as the apex angle of a cone with origin at the metal center with spreading edges along the van der Waals spheres of the outermost atoms (Figure 1).[8] Although its wide acceptance and constant use, this parameter has been flawed since its creation in the late 1970s. Originally, the Tolman cone angle was developed for symmetric monodentate phosphine ligands bound to a nickel center in a tetrahedral arrangement. The Ni–P distance was fixed to 2.28 Å, which is an average distance obtained from crystal structures, and the cone angle was measured using a physical space-filling model and a specialized ruler. In the case of asymmetric phosphine ligands the cone angle can be estimated by averaging the three angles between the phosphorus substituents: $\theta = 1/3\ (\theta_1 + \theta_2 + \theta_3)$.

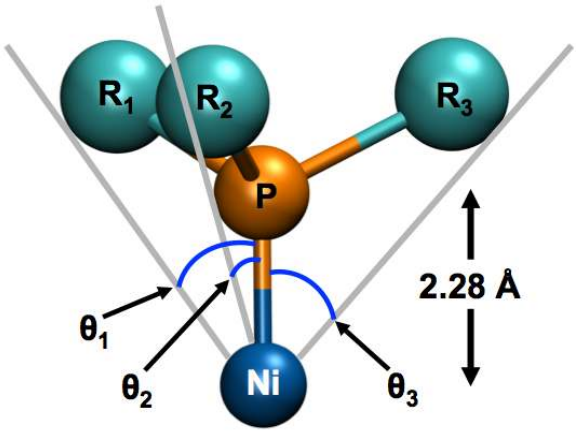

Figure 1. Ni–PR_3 model to measure the Tolman cone angle.

The main problem of this method is that ligand conformations are not taken into account when measuring the cone angle. In fact, in the original work by Tolman the ligands were folded up to make the smallest possible cone, without considering the relative stability of other possible structural alternatives. Therefore the original procedure works for small ligands *e.g.* PH_3 or PMe_3, but largely fails for ligands with bulkier and/or flexible substituents, meaning that the Tolman cone angle value is underestimated for most ligands. Although there were some late corrections using X-ray

structures, the Tolman cone angles have only been properly determined or calculated for some selected examples.[9]

Different steric measures, often employed in catalyst design procedures, have been developed since Tolman's cone angle proposal, and those have been reviewed by several authors.[10] These steric descriptors include solid angles (Θ)[11], the Ligand Knowledge Basis (LKB) steric He_8 descriptor,[12] the angular symmetric deformation coordinate (S_4')[13] and the percent buried volume descriptor ($\%V_{bur}$).[14] The Sterimol descriptors,[15] which were originally not developed as a steric measure, have been successfully employed to account for ligand bulkiness in quantitative structure−activity relationships in drug design and catalytic processes.[16] Alternatively, other procedures, mostly related to computational chemistry methods, have been developed to derive new values for the Tolman cone angles. The usage of DFT-optimized structures as source for obtaining cone angles has been carried out by different research groups, and new methodologies such as AARON[17] and Solid-G,[9a, 18] have been reported. Much in the same way, other options to generate θ values consist of mapping the average local ionization energy of ligands[19] or using data generated from a molecular mechanics approach.[20]

Due to nowadays computer power, which allows for accurate yet fast calculations on lots of molecules, a systematic and accurate approach to computing Tolman cone angles can be envisioned. To this end we have developed force fields able to screen for a great number of P-ligand (**P**) conformations in tetrahedral [$Ni(CO)_3$(**P**)] complexes. The best candidates, this is, those with the lowest relative energies, have been identified, and a DFT geometry optimization was performed on them. These two procedures are carried out without any structural constraint *i.e.* the Ni–P distance is no longer kept fixed at a value of 2.28 Å. From the optimized geometry, the Tolman cone

angle in a tetrahedral coordination environment (θ_T) is extracted with the FindConeAngle tool developed by Allen and coworkers,[21] currently implemented for Mathematica.[22] This method is fast and reliable, and allows the determination of the Tolman cone angle in any coordination environment without any of the assumptions made in the original cone angle development. The same research group has also reported a parallel procedure to obtain the exact solid angles (Θ)[11a] for a wide range of mono- and polydentate ligands.[23] Additionally, and since the cone angle should be responsive to the coordination environment of the ligand, the methodology described above has been extended to compute the phosphine cone angles in linear [AuCl(**P**)] (θ_L) and octahedral [$IrCl_3(CO)_2$(**P**)] (θ_O) complexes (Figure 2). The relative ligand arrangement in the latter complex corresponds to the one that minimizes the *trans* influence of the substituents on the iridium atom and consequently produces the lowest energy substitutional isomer.

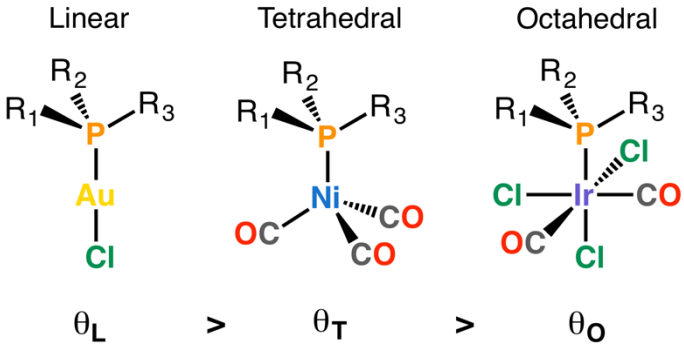

Figure 2. Computed transition metal complexes bearing a P-ligand and the expected influence of the coordination environment on the Tolman cone angle value.

Changing the coordination environment allows for the evaluation of the steric effects introduced by the ligand in different situations that may be important when studying organometallic reactions and catalytic processes. The three Tolman cone angles: θ_L, θ_T and θ_O, have been computed for 119 different monodentate P-ligands.

This set of structures includes the prototypical PR_3, PX_3, $P(OR)_3$, plus some of their combinations, and also the most representative ligands in catalytic processes, including many of the Buchwald biaryl ligands,[24] for which the cone angle has never been determined. Finally, the computed Tolman cone angles will be compared to a) previously reported values, b) other typical P-ligand steric measures found in literature such as solid angles (Θ),[11a] the LKB steric He_8 descriptor[12] and the angular symmetric deformation coordinate (S_4'),[13] and c) recomputed percent buried volumes ($\%V_{bur}$),[14] obtained from the lowest energy conformers found herein.

2. Computational details

As mentioned above, one of the problems that we face when trying to compute phosphine cone angles is the wide range of configurations that they can adopt. This is particularly critical in bulkier ligands with aliphatic groups, in which the flexibility may lead to several possible conformations, thus leading to multiple values for the corresponding cone angle. To perform an optimal screening of all possible configurations, and select among them the lowest energy ones, we performed a molecular mechanics (MM) screening using a generic linear dicoordinated [AuCl(**P**)] molecule, where **P** corresponds to all the P-ligands in Table 1. Using the DL_POLY Classic software for Molecular Mechanics,[25] a 1 ns trajectory in the NVT ensemble at 300 K has been done for all [AuCl(**P**)] systems (see SI for force field details). The corresponding outputs from the simulation have been later analyzed in order to extract the 10 lowest energy configurations across the trajectory. The lowest energy geometry has been used as a starting geometry the Density Function Calculations (DFT). This procedure was repeated for the tetrahedral [$Ni(CO)_3$(**P**)] and octahedral [$IrCl_3(CO)_2$(**P**)] complexes.

After the conformational ligand screening, the lowest energy structures have been fully optimized with the ωB97xD[26] functional as implemented in the Gaussian09 electronic structure suite.[27] In this process the C, N, O, F, P and H atoms are described with the TZVP[28] basis set while the Stuttgart basis set (SDD),[29] along with the corresponding ECPs, is employed for the Au, Ni, Ir, Cl, Br and I atoms. The density functional method has been selected following a benchmarking procedure in where the crystal structure of [AuCl(PMe_3)] was reproduced. Fifteen different functionals, some of them including the D3 dispersion correction of Grimme,[30] were tested for this purpose: B3LYP(D3),[31] BP86(D3),[32] PBE(D3),[33] PBE0(D3),[33-34] M06-2X(D3),[35] PW91,[36] TPSSh,[37] B97D,[38] B97D3[38a, 38b, 39] and ωB97xD. All the employed functionals produce very similar results, with errors below 3% in the Au–P, Au–Cl and P–C distances, and essentially the same Tolman cone angle (θ_L = 122.3 ± 0.4°). The final choice, ωB97xD, was done for two different reasons; 1) it has been shown to accurately reproduce the geometry of transition metal complexes[40] and 2) includes a version of the Grimme's dispersion model in its original formulation. The dispersion correction may not be relevant when optimizing a small species such as [AuCl(PMe_3)] but, as the size and complexity of the P-ligand increases, it may become a dominant term in the ligand final conformation *e.g.* for the bulkier and flexible biaryl ligands.

The final Tolman cone angles for the studied P-ligands, in the three different coordination environments, are extracted from the computed lowest-energy conformer geometry obtained with the described MM/DFT methodology using the FindConeAngle[21] package as implemented in Mathematica,[22] which employs the Bondi van der Waals radii[41] to describe the atoms size. The $\%V_{bur}$ calculations have been carried out with the Salerno molecular buried volume calculation (SambVca 2.0)[42] web applet. Three $\%V_{bur}$ values have been computed for every ligand, one for each

coordination environment: linear ($\%V_{bur-L}$), tetrahedral ($\%V_{bur-T}$) and octahedral ($\%V_{bur-O}$). In all cases the sphere radius has been kept fixed at 3.5 Å, the mesh spacing for numerical integration has been set to the default 0.1 value and the atomic radii employed correspond to the Bondi van der Waals radii scaled by 1.17. The optimized structures have been fed to SambVca, along with their corresponding M–P distances. As suggested in ref. 42, in most cases the H atoms have been ignored; exceptions to this are the ligands bearing H atoms on the phosphorus, for which the calculations of $\%V_{bur}$ have been carried out keeping those H atoms and deleting all the others.

3. Results and discussion

The computed Tolman cone angles, obtained from the lowest-energy structures for the linear [AuCl(**P**)] (θ_L), tetrahedral [$Ni(CO)_3$(**P**)] (θ_T) and octahedral [$IrCl_3(CO)_2$(**P**)] (θ_O) complexes, are shown in Table 1. The originally proposed cone angle values have been also included when available. As proposed, the computed cone angle responds to the coordination environment of the phosphine ligand. In most cases, the cone angle value decreases when the size of the metal fragment increases, *i.e.* when moving from the linear complex to the more hindered tetrahedral and octahedral structures ($\theta_L > \theta_T > \theta_O$). Most of the flexible phosphines and phosphites ligands, *i.e.* PR_3, PR_2R' and $P(OR)_3$, show this behavior, and a careful analysis reveals that the cone angle decrease is not related to a change in the ligand conformation, which actually remains unchanged. Some representative examples of ligands showing such behavior are P*t*Bu_3 (#7), PPh_3 (#11), PMe_2Et (#74), P*i*$PrPh_2$ (#100), $P(OEt)_3$ (#29) and $P(ONp)_3$ (#34). For all these ligands, the cone angle decrease seems just a response to the increasing congestion introduced by the metal complex. On the other hand, the smaller ligands such as PH_3 (#1), PMe_3 (#2), PH_2Me (#61), $PHMe_2$ (#67) and PX_3 (where X = F

(#20), Cl (#21), Br (#22) and I (#23)) show very similar cone angle values independently of the coordination environment. This should not be surprising at all given their small size, which entails also a complete absence of conformational noise. Obviously, the above trends are not always maintained and some outliers can be found when comparing the cone angle of a given ligand in the three coordination environments. An abrupt change in the computed cone angle is observed when varying the geometry of the metal complex in some cases; this behavior is normally related to a change in the ligand most stable conformation, which is triggered by the increasing steric hindrance of the higher coordination metal fragments. A couple of representative examples of this behavior are the PMe_2Bn (#81) and $PNpPh_2$ (#113) ligand, that present computed cone angles of 163.2, 159.5 and 123.9°, and 180.9, 148.5 and 146.4° in their respective [AuCl(**P**)], [$Ni(CO)_3$(**P**)] and [$IrCl_3(CO)_2$(**P**)] complexes. These numbers indicate that the most stable conformation of PMe_2Bn changes when the [$Ni(CO)_3$] fragment is replaced by [$IrCl_2(CO)_3$] –possibly because of the reorientation of the benzyl substituent– while in the case of $PNpPh_2$ the conformational change happens when the [AuCl] fragment is replaced by [$Ni(CO)_3$]. These results indicate that the latter ligand should have a larger steric influence, in agreement with the computed cone angle values. The Buchwald and other bulky biaryl P-ligands (Table 1, entries 36-60, structures shown in Table S1) show a similar behavior, which is often invoked to rationalize the reaction mechanism of catalytic homogeneous processes. These ligands present two different –- and characteristic– most likely conformations depending of the orientation of the secondary aryl ring, which may be pointing away (open conformation) or towards (close conformation) the metal center, establishing a metal–arene interaction (Figure 3).

Table 1. Original (**θ**) and computed ligand cone angles (in degrees) in different coordination environments: θ_L : [AuCl(**P**)], θ_T = [Ni(CO)$_3$(**P**)], θ_O = [IrCl$_3$(CO)$_2$(**P**)].

#	Ligand	θ	θ_L	θ_T	θ_O	#	Ligand	θ	θ_L	θ_T	θ_O
1	PH_3	87	105.1	106.4	101.0	61	PH_2Me		112.0	113.0	110.0
2	PMe_3	118	121.7	120.5	122.1	62	PH_2Et		135.3	136.0	126.0
3	PEt_3	132	167.7	169.0	157.8	63	PH_2iPr		136.2	134.2	128.7
4	PPr_3	132	167.7	169.1	157.7	64	PH_2tBu		136.6	134.5	128.9
5	$PiPr_3$	160	174.1	170.1	163.1	65	PH_2Np		114.3	115.7	114.0
6	PBu_3	132	168.6	171.5	160.6	66	PH_2Ph	101	140.3	140.2	120.7
7	$PtBu_3$	182	187.7	183.7	167.1	67	$PHMe_2$		120.2	119.0	120.8
8	PNp_3	180	198.3	170.2	155.0	68	$PHEt_2$		145.8	144.7	141.7
9	$PCyp_3$		178.6	165.2	161.5	69	$PHiPr_2$		143.6	142.2	130.6
10	PCy_3	170	176.3	174.7	164.9	70	$PHtBu_2$		174.4	169.9	162.8
11	PPh_3	145	168.0	165.8	152.0	71	$PHNp_2$		157.9	166.3	152.8
12	P(*o*-Tol)$_3$	194	190.3	183.4	175.6	72	$PHAd_2$		175.6	171.3	164.2
13	P(*o*-ClC$_6$H$_4$)$_3$		189.9	184.7	173.7	73	$PHPh_2$	128	148.1	147.2	139.2
14	P(*p*-Tol)$_3$	145	167.9	165.7	152.1	74	PMe_2Et	123	143.9	142.6	138.5
15	P(*p*-ClC$_6$H$_4$)$_3$	145	168.3	166.0	152.0	75	PMe_2Pr		144.1	142.8	138.3
16	P(3,5-Me$_2$C$_6$H$_3$)$_3$		177.1	170.8	164.9	76	PMe_2iPr	132	147.6	146.7	140.6
17	P(3,5-Cl$_2$C$_6$H$_3$)$_3$		170.2	169.2	160.6	77	PMe_2tBu	139	147.0	145.9	143.2
18	P(naph)$_3$		189.9	184.2	173.1	78	PMe_2Np		131.1	130.3	129.7
19	PBn_3	165	187.5	165.9	153.3	79	$PMeAd_2$		176.1	171.4	165.7
20	PF_3	104	108.5	114.9	104.7	80	PMe_2Ph	122	149.6	147.8	133.2
21	PCl_3	125	118.5	119.0	116.4	81	PMe_2Bn		163.2	159.5	123.9
22	PBr_3	131	123.4	123.6	120.7	82	$PMeEt_2$	127	142.8	141.5	137.5
23	PI_3		129.6	129.1	125.7	83	$PMePr_2$		142.8	141.4	137.1
24	P(CF$_3$)$_3$	137	135.0	141.6	139.1	84	$PMeiPr_2$	146	170.1	166.4	160.1
25	P(CCl$_3$)$_3$		172.6	171.7	159.3	85	$PMetBu_2$	161	174.5	169.9	165.2
26	P(C$_2$F$_5$)$_3$		173.9	173.5	165.3	86	$PMeNp_2$		165.5	161.3	151.0
27	P(C$_6$F$_5$)$_3$	184	177.9	172.5	159.3	87	$PMePh_2$	136	152.4	147.4	142.3
28	P(OMe)$_3$	107	168.8	156.8	153.0	88	$PMeBn_2$		183.9	178.5	145.2
29	P(OEt)$_3$	109	171.1	170.7	152.6	89	PMeEtPr		142.9	141.5	137.3
30	P(OPr)$_3$		187.6	178.5	155.1	90	PEt_2Pr		155.2	145.4	140.0
31	P(O*i*Pr)$_3$	130	183.0	172.5	146.0	91	PEt_2Ph	136	157.6	155.7	139.4
32	P(OBu)$_3$	110	196.6	179.4	153.4	92	PEt_2Bn		184.9	180.2	145.8
33	P(O*t*Bu)$_3$	172	200.9	176.0	157.7	93	$PEtPr_2$		155.2	154.6	142.2
34	P(ONp)$_3$		187.6	166.1	147.7	94	$PEtPh_2$	140	168.3	152.8	148.2
35	P(OPh)$_3$	128	168.8	152.9	130.5	95	$PEtBn_2$		171.7	168.8	154.4
36	BrettPhos		251.3	191.4	181.6	96	$PiPr_2Cy$		176.3	173.2	164.5
37	*t*BuBrettPhos		250.9	196.9	182.3	97	$PiPrCy_2$		176.0	174.7	164.2
38	CataCxium-PCy		216.6	175.8	179.7	98	$PiPrAd_2$		181.8	177.1	169.2
39	CataCxium-POMeCy		221.2	176.4	163.2	99	$PiPr_2Ph$		172.7	169.1	162.4
40	CataCxium-POMetB		224.0	183.3	168.1	100	$PiPrPh_2$	150	174.3	170.8	156.6
41	CataCxium-PtB		225.2	183.4	168.0	101	$PiPr_2Bn$		181.9	177.9	172.7
42	CPhos		214.7	177.6	164.2	102	$PiPrBn_2$		186.9	181.4	171.0
43	DavePhos		211.2	173.2	164.4	103	PAd_2Bu (CataCxium-A)	176	180.6	176.3	169.2
44	*t*BuDavePhos		228.1	188.5	172.7	104	$PtBu_2Cy$		182.0	177.4	168.6
45	PhDavePhos		206.9	161.3	155.6	105	$PtBu_2Ph$	170	186.9	182.7	167.7
46	JackiePhos		236.2	194.2	193.6	106	$PtBu_2Bn$		196.7	188.9	177.4
47	JohnPhos		228.9	184.1	166.7	107	$PtBuCy_2$		181.8	178.4	169.4
48	CyJohnPhos		208.0	176.4	164.8	108	$PtBuAd_2$		188.9	184.6	173.0
49	MePhos		208.9	174.4	165.3	109	$PtBuPh_2$	157	168.5	163.9	155.6

50	*t*BuMePhos	228.9	183.8	160.8	110	P*t*BuBn$_2$		194.6	169.7	166.3
51	MeDalPhos	214.7	185.7	170.4	111	PNp$_2$Ph		185.7	179.9	171.7
52	MorDalPhos	231.2	186.5	173.4	112	PNp$_2$Bn		194.3	179.6	173.0
53	RuPhos	231.5	205.5	212.7	113	PNpPh$_2$		180.9	148.5	146.4
54	SPhos	227.4	204.4	201.7	114	PNpBn$_2$		200.7	182.8	159.8
55	XPhos	238.7	173.3	172.2	115	PCy$_2$Ph	159	172.6	169.0	162.2
56	*t*BuXPhos	250.6	178.6	178.9	116	PCyPh$_2$	152	174.3	170.4	158.2
57	cBridP	226.0	210.0	198.3	117	PAd$_2$Bn (CataCxium-Abn)		198.3	189.3	165.2
58	CycBridP	224.3	204.2	194.1	118	PPh$_2$Bn	152	188.6	169.6	165.5
59	vBridP	227.4	210.9	201.3	119	PBn$_2$Ph		189.9	181.9	171.3
60	CyvBridP	211.1	192.8	174.6						

Me = methyl, Et = ethyl, Pr = propyl, *i*Pr = *iso*propyl, Bu = butyl, *t*Bu = *tert*butyl, Np = neopentyl, Cyp = cyclopentyl, Cy = cyclohexyl, Ad = 1-adamantyl, Ph = phenyl, Bn = Benzyl, Tol = tolyl, naph = 1-naphthyl.

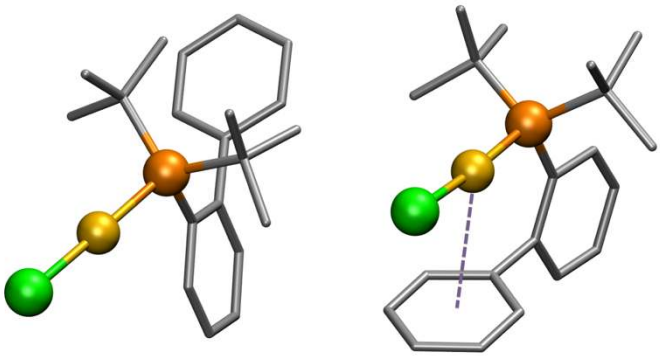

Figure 3. Schematic representation of the biaryl P-ligand displaying the open (left) and close (right) conformations in [AuCl(**P**)] complexes (color code: Au = yellow, P = orange, Cl = green, C = gray, for clarity H atoms have been omitted).

Obviously, the latter conformation is only possible when the metal fragment displays a low coordination number, as in the studied [AuCl(**P**)] linear complexes. Both conformations have been computed for the gold complexes of the biaryl ligands in order to compare the energy differences and the cone angle values (Table S2). In all cases, the lowest-energy structures correspond to those displaying the close conformation, in which the shortest contact between the gold atom and the dangling group of the biaryl substituent (usually a carbon atom) is found at distances ranging from 3.10 to 3.40 Å. These distances are, in most cases, shorter than the sum of van der Waals radii of the interacting atoms: Au (1.66 Å) and C (1.70 Å). In the case of MeDalPhos, (#51) the distance between the gold atom and the N,N-dimethylaniline substituent is as short as

2.87 Å, mainly due to the strong donor ability of the dangling amine group. The average energy difference between the close and open conformations for these 25 ligands is around 7.2 (±3.3) kcal mol^{-1}, always in favor of the former. Pulling the bulky biaryl substituent away from the metal center in [AuCl(**P**)] complexes, and hence getting to the higher energy open conformation, produces a less strained geometry and a huge decrease in the cone angle value. The average cone angle difference between both conformations is 35.2 (±13.5)° always in favor of the –more energetically stable– close conformation. Figure 4 shows the difference between the computed cone angles with respect to the smallest cone angle for each ligand.

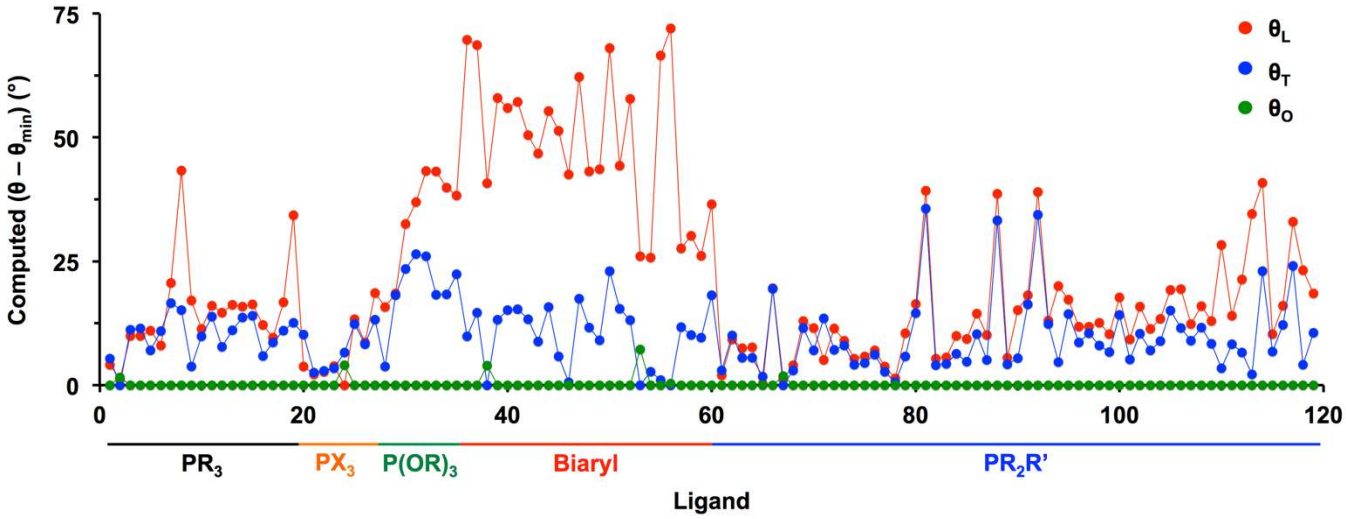

Figure 4. Relative differences between computed linear (θ_L), tetrahedral (θ_T) and octahedral (θ_O) cone angles.

As may be observed (Table 1), the minimum cone angle value is found for octahedral $[IrCl_3(CO)_2(\mathbf{P})]$ complexes, in 114 ligands out of 119, in agreement with the predicted trend. Following this tendency, the tetrahedral complex $[Ni(CO)_3(\mathbf{P})]$ shows a smaller cone angle than the linear [AuCl(**P**)] counterpart for 108 of the studied ligands. Only in one case the latter geometry is found to produce the smallest cone angle; the $P(CF_3)_3$ ligand (#24) has cone angles of 135.0, 141.6 and 139.1° for the linear,

tetrahedral and octahedral complexes respectively. These differences, although not very important in absolute numbers, cannot be justified by a change in the ligand conformation, and can only be explained by the variation of the M–P distances observed for $P(CF_3)_3$ in the studied complexes. The M–P distance in the linear and octahedral compounds is 2.24 and 2.33 Å, respectively, whereas in the Ni complex it becomes much shorter (2.16 Å) and thus produces a slightly larger cone angle. The extremely electron-poor donating character of the $P(CF_3)_3$, combined with the Ni(0) oxidation state, is probably helping in the shortening of the Ni–P distance. In fact, the M–P distances, which are allowed to change during the geometry optimization procedure, may have a certain impact in the final cone angles (*vide infra*). On the other hand, five ligands: PMe_3 (#2), CataCxium-PCy (#38), RuPhos (#53), *t*BuXPhos (#56) and $PHMe_2$ (#67), show the smallest cone angle in their tetrahedral [$Ni(CO)_3$(**P**)] complexes. In the case of PMe_3 and $PHMe_2$ the difference between the computed cone angle values is very small (*ca.* 1.5°) and does not seem to be significant. The other three ligand showing this behavior belong to the biaryl subclass; in the case of CataCxium-PCy and *t*BuXPhos the difference between the [$Ni(CO)_3$(**P**)] and [$Ir(Cl_3(CO)_2$(**P**)] cone angles is as small as 3.9 and 0.3°, respectively, which could be attributed to the relative orientation of the ligand substituents and their dispersive interaction with the ligands on the metal fragment. Finally, in the case of RuPhos, one of the dangling O^{i}Pr substituents on the biaryl ring suffers a small reorganization when going from the tetrahedral to the octahedral arrangement, which probably entails a stronger interaction with the carbonyl ligands and the iridium atom, and a slightly different cone angle value. Of course, there are other cases that would deserve a more complete study but, at this point, we believe it is better to keep an eye on the general trend than focusing on the particularities of each ligand. The main conclusion extracted from the comparison between the linear (θ_L), tetrahedral

(θ_T) and octahedral (θ_O) cone angles is that, as expected, the cone angle becomes smaller (*i.e.*, $\theta_L > \theta_T > \theta_O$) as the coordination number of the metal increases.

The computed cone angles can be compared with the 44 available Tolman cone angle values (Figure 5). In general, the computed cone angles present larger values than those proposed by Tolman, especially in the case of the less sterically demanding linear gold complex (Figure 5, left). This should not be surprising because of the cone angle original formulation, in which the smallest possible ligand conformation was chosen. The overall correlation between the computed and measured cone angles is not good in any case, although θ_O seems to provide a better approximation. Nevertheless, similar average cone angles can be found for some species such as PMe_3, PCy_3, P*t*Bu_3, PNp_3 and PAd_2Bu. Interestingly, the smallest phosphine ligand PH_3 produces significantly larger cone angles when compared to the original value: $\theta_L = 105.1°$, $\theta_T = 106.4°$, $\theta_O = 101.0°$, $\theta = 87°$. The analysis of cone angles can be also done for the different ligand classes; for instance, when comparing θ and θ_O for the PR_3, PX_3, $P(OR)_3$ and PR_2R' ligand families, average errors of 10, 6, 24 and 6 % are obtained, respectively. These values clearly indicate that the phosphite family was not particularly well described by the original cone angle formulation. However, leaving the $P(OR)_3$ ligands out of the θ_O *vs.* θ correlation produces only a slight improvement in the correlation ($\theta = 0.67\theta_O + 50.78$, $R^2 = 0.780$), which indicates that other compounds may also be problematic.

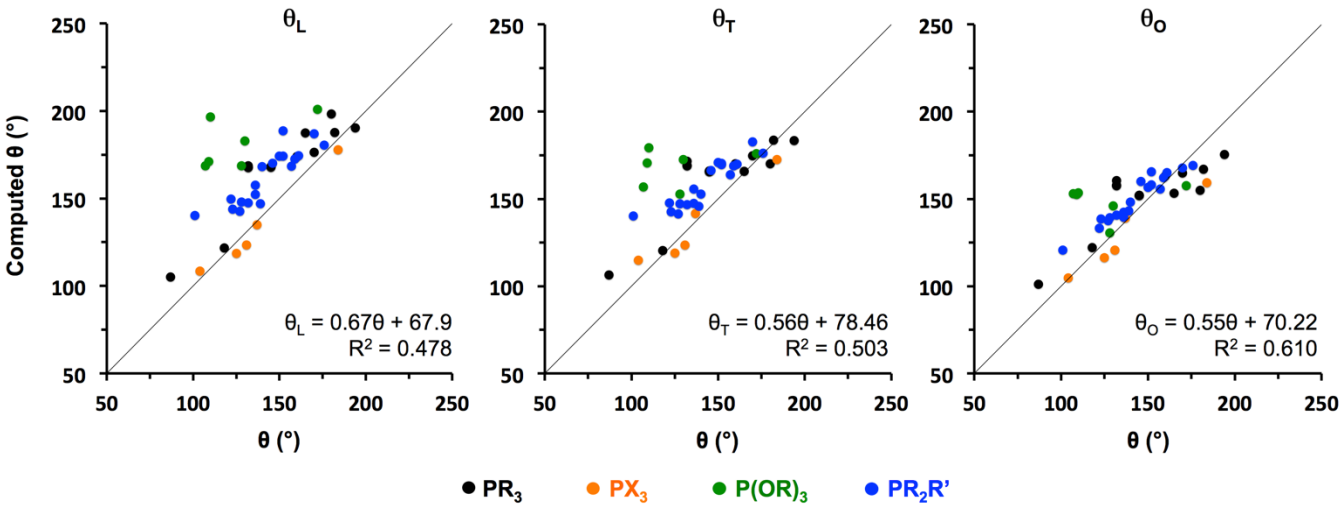

Figure 5. Correlation of original and computed Tolman cone angles (θ) for linear [AuCl(**P**)] (θ_L), tetrahedral [Ni(CO)$_3$(**P**)] (θ_T) and octahedral [Ir(Cl$_3$(CO)$_2$(**P**)] (θ_O) coordination environments. The data color code represents the different ligand classes.

In contrast to the classical Tolman cone angle formulation, the MM/DFT methodology employed here does not add any structural constraint, *i.e.*, we do not keep the M–P distance fixed at 2.28 Å. In practice this should have a certain impact in the computed cone angles, mostly related to the electronic properties of the ligand, meaning that under similar steric hindrance conditions, the electron-poor ligands should produce shorter M–P distances. Indeed, this is observed for ligands such as PMe$_3$ (#2) and PBr$_3$ (#22). Both these ligands have quite similar θ_L, θ_T and θ_O values but the M–P distances for the latter are always shorter, in particular by 0.03, 0.08 and 0.01 Å in the linear, tetrahedral and octahedral arrangements, respectively. In any case, the M–P distances found do not differ much from the original 2.28 Å value; the average Au–P, Ni–P and Ir–P distances are 2.28, 2.26 and 2.39 Å and their standard deviations remain below 0.05 Å, indicating a relatively low dispersion. The effect of the M–P distance in the final values of the cone angles is limited, and differences between the Tolman cone angle and the computed analogs should only be expected to appear when the computed distances move away from 2.28 Å. As an example, θ_L has been recomputed at an Au–P distance of

2.28 Å for some of the ligands showing the largest distance deviations: P*t*Bu$_3$ (#7), P(*o*-Tol)$_3$ (#12), PF_3 (#20), P(CF$_3$)$_3$ (#24), P(OPh)$_3$ (#35), and *t*BuBrettPhos (#37). These recomputed $\theta_{L(2.28)}$ values show an average variation of only 1.5°. Obviously, $\theta_L > \theta_{L(2.28)}$ for the ligands having Au–P distances shorter than 2.28 Å, while the opposite effect ($\theta_L < \theta_{L(2.28)}$) is observed for those ligands with longer Au–P distances. In the case of θ_O, this effect is more pronounced. However, it is clear the most important contribution to the cone angle variation comes from conformational changes on the ligand rather than to the elongation of the Ir–P distance.

As stated above, the computed cone angles tend to be larger than those obtained with the classical formulation. Many times the difference between θ and the computed analogs is related to a conformational mismatch between the original –compressed– ligands and their optimized lowest energy conformers, which should be expected to produce larger cone angles. The [AuCl(**P**)] complexes –and their corresponding θ_L values– for some ligands in their compact conformation have also been calculated to assess the performance of the computational methodology (Table 2).

Table 2. Computed *vs.* compact conformer relative energies (E_{REL}, in kcal mol^{-1}) and θ_L values for the [AuCl(**P**)] complexes of some P-ligands. The original Tolman cone angle (θ) has been included when available.

	MM/DFT conformer		Compact conformer		
Ligand	E_{REL}	θ_L	E_{REL}	θ_L	θ
PEt_3	0.0	167.7	5.7	135.9	132.0
PPr_3	0.0	167.7	5.5	136.0	132.0
PMe_2Et	0.0	143.9	1.0	124.4	123.0
PMe_2Pr	0.0	144.1	1.1	124.6	-
$PMeEt_2$	0.0	142.8	2.6	129.3	127.0
P(OMe)$_3$	0.0	168.8	8.3	110.1	107.0
P(OEt)$_3$	0.0	171.1	8.5	126.9	109.0

As may be observed, the combined MM/DFT sequence produces lower energy structures than those in which the ligand is optimized in its compact conformation; the energy differences range between 1.0 and 8.5 kcal mol^{-1}, always in favor of the MM/DFT computational approach. The cone angles for this small subset of ligands show quite important differences between the computed θ_L parameters for the ligands in both conformations, and the values obtained with the MM/DFT method are always larger, with an average difference of +31°. These results clearly indicate that the new computed values should be a more representative description for the ligand sterics. On the other hand, the calculations on most of the compressed ligands produce similar cone angle values to those reported originally; with $P(OEt)_3$ giving the largest deviation because of the starting conformation chosen for the calculation, which was the most wrapped out structure, evolving into a more extended configuration.

One of the main concerns of the presented methodology is related, precisely, to the conformational flexibility of the ligands. How can we be sure that we are capturing the right conformer for each ligand in each coordination environment? Of course, one cannot be completely sure that automated protocols such as the one employed here provide with the correct answer in all cases. In addition, the use of molecular mechanics to screen for the lowest energy conformers for each ligand does not directly imply that the best structures found correspond to the most stable conformers onto the DFT potential energy surface. Nevertheless, we believe that our method may be capturing most of the lowest-energy structures. As an example, we show the relative energies of PEt_3 in different conformations in the two most extreme coordination environments: linear and octahedral. In both cases our automated force field exploration processes lead to the lowest energy conformer, which has a different arrangement of the dangling ethyl groups (Table 3). In the less strained linear complex PEt_3 preferentially adopts the most

spread out conformation (**F**) where the three alkyl substituents lay on a circular arrangement. Three other conformations, **C**, **D** and **E**, are found to produce similar [$AuCl(PEt_3)$] complexes in terms of energy (*ca.* 1 kcal mol^{-1}) and cone angles. On the other hand, in the octahedral [$IrCl_3(CO)_2(PEt_3)$] complex the most favored conformer displays a parallel arrangement between two ethyl groups while the third one points away from the metal (**D**). This complex has also the highest value for the cone angle (157.8°). In this case all the other conformers exhibit higher energies (at least 1 kcal mol^{-1}) and significant lower cone angle values.

Table 3. Conformer analysis for the [$AuCl(PEt_3)$] and [$IrCl_3(CO)_2(PEt_3)$] complexes. E_{REL} is the relative energy difference (in kcal mol^{-1}) between the conformer and its lowest energy analog. Gray balls indicate methyl groups pointing outwards.

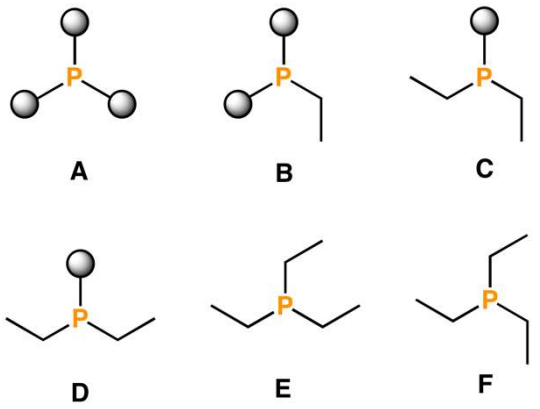

	[$AuCl(PEt_3)$]		[$IrCl_3(CO)_2(PEt_3)$]	
Conformer	E_{REL}	θ	E_{REL}	θ
A	5.7	135.9	3.8	133.5
B	2.7	148.5	1.0	141.7
C	0.4	155.3	1.2	145.0
D	0.1	165.1	0.0	157.8
E	0.7	169.8	2.9	153.3
F	0.0	167.7	2.3	146.9

The octahedral computed cone angle (θ_O) has been compared (Figure 6) with other available phosphine steric parameters such as the solid angles (Θ),[11a] the LKB-P steric descriptor He_8,[12b-d] the angular symmetric deformation coordinate (S_4'),[13] and the percent buried volumes ($\%V_{bur}$, Figure 7).[14] A complete list of values for these quantities can be found in the ESI (Table S3). Very similar correlations are obtained when comparing the linear (θ_L) and tetrahedral (θ_T) cone angles, and therefore those have not been included. The correlation between θ_O and the solid angle Θ, for which 24 values are available, is quite similar and equally imprecise to that found with the original Tolman cone angle. Most computed θ_O values are larger than the corresponding solid angles and the correlation coefficient is as low as $R^2 = 0.456$. These results are not surprising, and this is because of the formulation of the solid angle. The classical estimation of Θ deals partially with the conformational issue of the ligand and minimum/maximum values are usually derived; of course, this process does not take into consideration the relative energies of the metal–ligand complexes. In addition, the determination of Θ entails once again fixing the M–P distance at 2.28 Å, which introduces some inaccuracies in the final values.

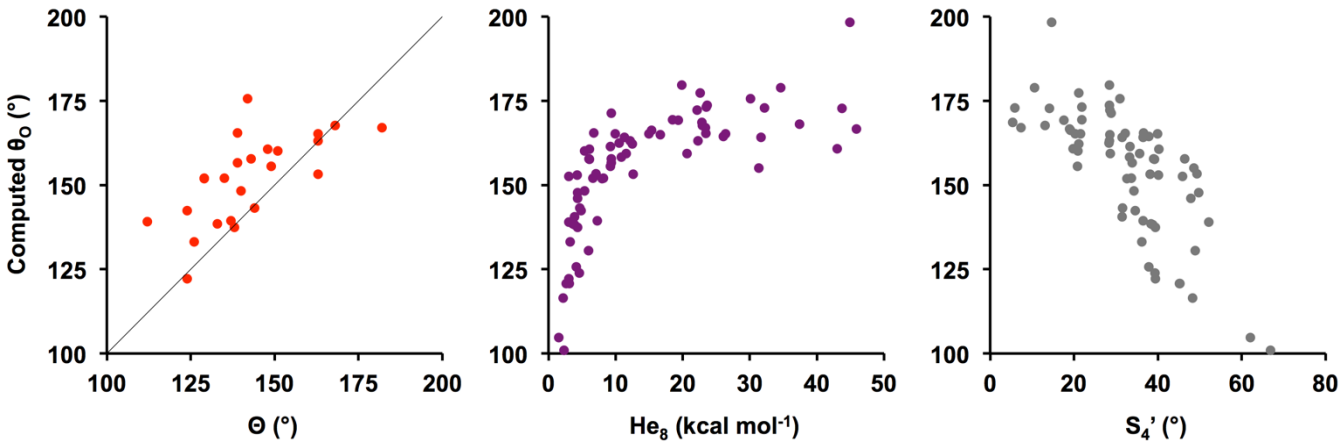

Figure 6. Correlation between the computed octahedral cone angle (θ_O) and different steric measures for P-ligands: solid cone angles Θ (left), Ligand Knowledge Base (LKB) He_8 (middle) and angular symmetric deformation coordinate S_4' (right).

The monodentate phosphine Ligand Knowledge Base (LKB-P) contains the steric descriptor He_8.[12a, 12b] This descriptor is calculated as the interaction energy between a P-ligand and a ring of 8 He atoms, which remain fixed in a regular distribution on a circle of radius 2.5 Å. As in the Tolman cone angle, the distance between the P atom and the centroid of the He_8 ring is kept frozen at 2.28 Å. This setup aims to mimic the interaction between the P-ligand and other *cis*-coordinated groups in an octahedral complex. One of the cons of employing He_8 is that its interpretation is not immediate and sometimes is difficult to think of an energy value as a steric measure of a ligand. As may be observed the correlation between θ_O and He_8 is not good, *e.g.*, ligands such as $P(Np)_3$ (#8) and P^tBuPh_2 (#109) have practically the same θ_O value while the He_8 parameter differs by more than 20 kcal mol^{-1}. In addition, strong deviations start to appear when the size of the ligand increases over 150°, probably because of conformational inconsistencies derived from the original LKB calculations. Another plausible explanation for the deviations observed in larger ligands is the unavoidable approximation of the ligand dangling substituents to the He ring, which ends up producing larger interaction energies than expected. Another steric ligand measure for phosphines is the angular symmetric deformation coordinate S_4'.[13] This parameter is defined as the sum of the M–P–R angles (α_i) minus the sum of the R–P–R angles (β_i) in a given metal–phosphine complex, which can be related to the flattening or pyramidalization of the ligand. In addition, S_4' does not include any reference to the geometry of the dangling atoms in each of the R substituents. The correlation of θ_O and S_4' shows a quite large scattered distribution with a subtle negative tendency, *i.e.*, smaller S_4' values produce larger θ_O, as proposed originally. This relationship indicates that phosphines with a small cone angle will give a large M–P–R and a small R–P–R sums. Therefore, the phosphine becomes then more pyramidal. Conversely, if the M–P–

R sum decreases and the R–P–R sum increases the ligand gets flattened and the cone angle will be larger. However, the results obtained do not outline a clear relationship between the computed θ_O and S_4' parameters.

Finally, the computed linear (θ_L), tetrahedral (θ_T) and octahedral (θ_O) cone angles can be compared to their corresponding percent buried volumes[14] ($\%V_{bur\text{-}L,}$ $\%V_{bur\text{-}T}$ and $\%V_{bur\text{-}O}$, respectively). In principle, there is not any database containing the "right" $\%V_{bur}$ values for phosphine ligands, therefore $\%V_{bur}$ values have to be computed for each of our optimized structures, employing the SambVca[42] web applet. The values for the three $\%V_{bur}$ quantities can be found in Table S3. The correlation between the computed θ and $\%V_{bur}$ are moderately good in all cases; Figure 7 shows the best correlation, obtained between θ_L and $\%V_{bur\text{-}L}$ (correlations between the tetrahedral and octahedral analogs can be found in Figure S1). This correlation clearly indicates a positive relationship between θ_L and $\%V_{bur\text{-}L,}$ as should be expected. However, a deviation can be clearly appreciated for the smaller ligands, mainly those with θ_L < 130°, for which larger $\%V_{bur}$ values than expected are found. Those ligands belong mostly to the PX_3 class, where X is an electronegative substituent (F, Br, Cl, I or CF_3). These electron-poor ligands produce a relatively short Au–P distances and takes most parts of the ligand into the 3.5 Å sphere employed to derive the $\%V_{bur}$, which in the end produces a larger steric hindrance. The same behavior is also observed for the same ligands in the computed $\%V_{bur\text{-}T}$ and $\%V_{bur\text{-}O}$ descriptors.

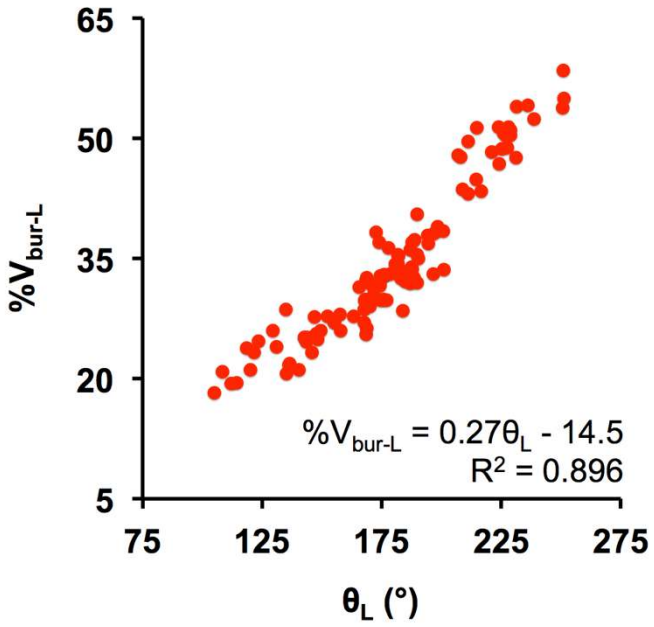

Figure 7. Correlation between the computed linear cone angle (θ_L) and its corresponding $\%V_{Bur\text{-}L}$ descriptor.

The cone angles computed herein should be employed in the same way as the original Tolman cone angle was used to model and predict the properties of systems in which phosphine ligands play a key role. Unfortunately, most of the available data in literature show a relatively good correlation with the Tolman cone angle and, since the relationship between the original θ and the ones computed here is not linear, those data cannot be employed. The main problem is that the information not correlating with the Tolman cone angle is practically non-existent in literature and thus finding examples where the new computed cone angles could be correlated with experimental data is not easy. Nevertheless, after doing some data mining, some examples could be found. The first one deals with the experimental phosphine dissociation enthalpies from open titanocene [Ti(2,4-C_7H_{11})$_2$(PR_3)] complexes (Scheme 1).[43] In the original report, the dissociation enthalpies were measured for six PR_3 ligands (PMe_3, PMe_2Ph, PPh_3, PF_3, $P(OMe)_3$ and $P(OEt)_3$), and found to not correlate well with the Tolman cone angle. This observation encouraged the authors to state that some cone angles, those of $P(OMe)_3$ and

$P(OEt)_3$, were wrong and led to a refining procedure that provided more adjusted cone angle values.

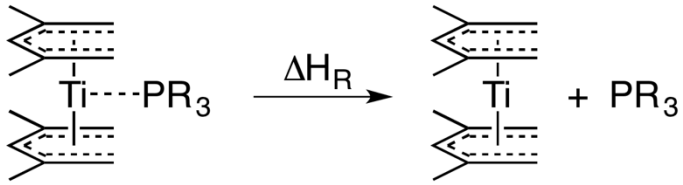

Scheme 1. Phosphine ligand dissociation (ΔH_R) from open titanocene [Ti(2,4-$C_7H_{11})_2(PR_3)$] complexes.

In contrast, the relationship between the phosphine dissociation enthalpies and the computed θ_O parameter is quite good (Figure 8). The determination coefficient found is $R^2 = 0.991$, showing a clear negative linear dependence between the phosphine dissociation enthalpy and the θ_O parameter, which indicates that larger P-ligands should produce lower dissociation enthalpies. The linear model can be also employed to predict the dissociation enthalpies for other ligands in Table 1; the results show that the ligand dissociation from the open titanocene fragment is endothermic ($\Delta H_R > 0$) for all the studied species, including those for which the linear regression model incurs into extrapolation *i.e.* ligands with θ_O larger than 153° (Table S4). The lowest dissociation enthalpies are found for bulky biaryl ligands such as RuPhos (#53), SPhos (#54) and vBridP (#59), which take values of 1.6, 3.1 and 3.2 kcal mol^{-1}. On the other hand, the highest dissociation enthalpy, 17.7 kcal mol^{-1}, is found for PH_3 (#1).

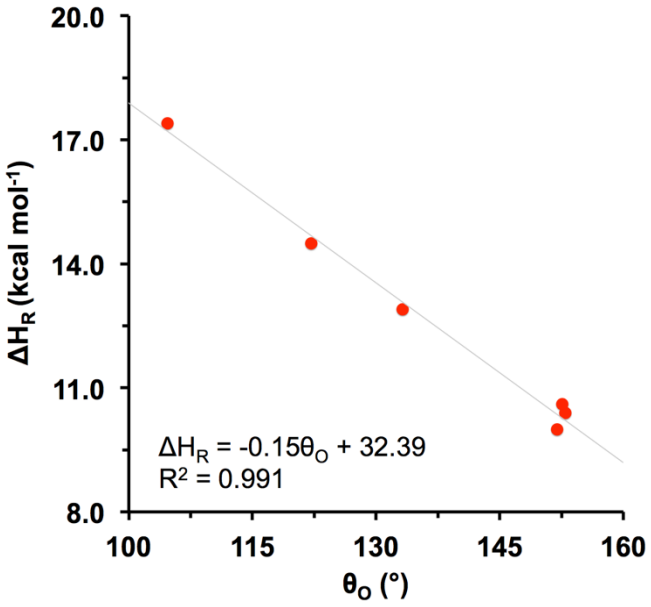

Figure 8. Correlation between the computed octahedral cone angle (θ_O) and the phosphine ligand dissociation enthalpies (ΔH_R, in kcal mol^{-1}) from open titanocene [Ti(2,4-C_7H_{11})$_2$(PR_3)] complexes.

Alternatively, the computed tetrahedral θ_T parameter (θ_L and θ_O produce similar results) can be employed to model DFT reaction barriers, *e.g.* those reported for the Suzuki-Miyaura reaction between bromobenzene and a monoligated [Pd-PR_3] catalyst (where PR_3 = $P(CF_3)_3$, PMe_3, P*t*Bu_3 and PPh_3, Scheme 2).[44] Of course, these reaction barriers depend both on the electronic and steric features of the ligand and thus multilinear regression relationships have to be developed. The electronic descriptors taken into consideration are the HOMO and LUMO energies of the free ligand, which can be related to the electron σ-donation and π-acceptance ability of the phosphine. Both these descriptors have been extracted from the monodentate phosphine Ligand Knowledge Base (LKB-P).[12b] The computed reaction barriers and the ligand descriptor values can be found in Table S5.

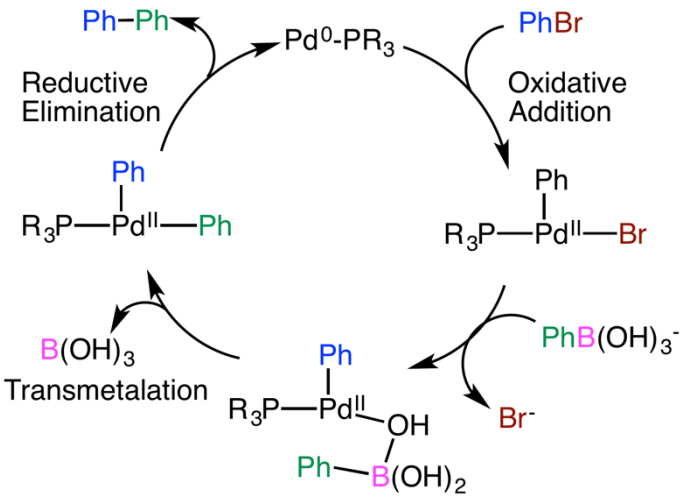

Scheme 2. General catalytic cycle for the Suzuki-Miyaura reaction between [Pd-PR_3] and bromobenzene.

It should be noted that a small structure set such as the one employed here, only 4 ligands, limits the statistical significance of the linear models. Nevertheless, these simple models provide the right trend when describing the barrier heights, and provide a good quantitative estimation into the ligand effects on each barrier. The three barriers in the Suzuki-Miyaura cross-coupling catalytic cycle: oxidative addition, transmetalation and reductive elimination, can be successfully modeled and show different dependence degrees on the ligand electronic and steric properties (Table 4).

Table 4. Multilinear models for computing the reaction barriers (in kcal mol^{-1}) in the Suzuki-Miyaura reaction between [Pd-PR_3] and bromobenzene. The employed descriptors are the tetrahedral cone angle θ_T (°), and the HOMO (E_{HOMO}) and LUMO (E_{LUMO}) energies (both in Hartrees) of the free phosphine ligand. The β parameters are the standardized regression coefficients of each descriptor.

Barrier	Barrier height =	R^2	$\beta(E_{HOMO})$	$\beta(E_{LUMO})$	$\beta(\theta_T)$
Oxidative Addition	$0.01\theta_T$ - $78.60E_{HOMO}$ - 12.48	0.999	-1.03	-	0.09
Transmetalation	$0.03\theta_T$ - $44.35E_{LUMO}$ + 12.77	0.974	-	0.93	0.39
Reductive Elimination	$-0.03\theta_T$ + $27.91E_{HOMO}$ +13.60	0.963	1.04	-	-0.63

As may be observed in Table 4, the major ligand effect on the oxidative addition barrier is related to the σ-donation ability, while the steric hindrance of the ligand has only a limited effect; the standardized regression coefficients of the HOMO energy and θ_T are -1.03 and 0.09, respectively, indicating that the former is almost 11 times more important. This should not be surprising since the reaction takes place on a quite unhindered monoligated palladium complex. The negative sign of the E_{HOMO} descriptor indicates that the stronger σ-donor ligands favor the Pd insertion in the C–Br bond, thus contributing in lowering the barrier for this reaction stage in agreement with previous reports.[45] The determination coefficient found for the oxidative addition multilinear regression is very high $R^2 = 0.999$, indicating an almost perfect match.

In the case of the transmetalation barrier a quite good multilinear regression model is also found ($R^2 = 0.973$) when employing the E_{LUMO} as the electronic acceptance character of the phosphine ligand; the usage of E_{HOMO} as electronic descriptor provided a poorer regression ($R^2 = 0.743$), and was consequently discarded. The transmetalation regression model shown in Table 4 states that the electronic factors are *ca.* 2 times more important than the sterics: $\beta(E_{LUMO}) = 0.93$ while $\beta(\theta_T) = 0.39$. The sign of the θ_T steric parameter is positive, which indicates that bulkier ligands should produce higher transmetalation barriers; this behavior could be related to the steric repulsion produced by the phenylboronate and the phosphine ligand in the process of ligand exchange. The sign of de E_{LUMO} descriptor is also positive, indicating that the more π-acceptor phosphines will lower the transmetallation barrier, probably by stabilizing the additional electron density on the metal.

The multilinear regression model for the reductive elimination barrier shows also a good determination coefficient ($R^2 = 0.963$), which states that E_{HOMO} and θ_T can be employed as descriptors to model this reaction step. The standardized coefficients of

both descriptors are $\beta(E_{HOMO})$ = 1.04 and $\beta(\theta_T)$ = -0.63, which show that both factors are important in the reductive elimination. The sign θ_T is negative, indicating that bulky phosphines will lower the reductive elimination barrier, probably by pushing the two phenyl groups closer and facilitating the biphenyl product formation. In contrast the sign of E_{HOMO} is positive, which means that stronger σ-donor ligands will be more prone to delocalize electron density on the metal center, hence producing a higher reductive elimination barrier. This regression model indicates that bulky and electron-poor phosphines produce the lowest reductive elimination barriers, as reported previously.[46]

In addition, the multilinear models shown above can be employed to predict the reaction barriers of the other ligands in Table 1, provided the electronic descriptors E_{HOMO} and E_{LUMO} can be found in the LKB-P database. Therefore, applying the multilinear regression models to the additional 64 available ligands allows generating electronic/steric ligand maps for each reaction barrier (Figure 9, see Table S6 for predicted barrier values), where the barrier height is projected in a bidimensional surface. It has to be noted that none of the predicted reaction barriers takes a negative value, not even in cases where the barriers had to be extrapolated.

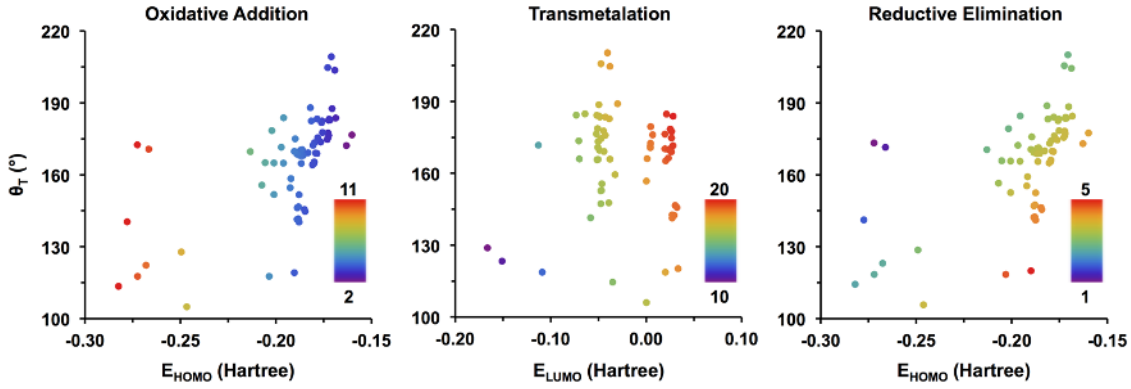

Figure 9. Projected oxidative addition, transmetalation and reductive elimination barriers (in kcal mol^{-1}) for the Suzuki-Miyaura reaction between [Pd-PR_3] and bromobenzene as a function of the electronic/steric features of the phosphine ligand. The barrier heights are represented in color code, where barrier values increase from purple to red tones.

As may be observed, the ligand maps reflect the impact of each descriptor in the oxidative addition, transmetalation and reductive elimination barrier heights. The multilinear regression for oxidative addition is nearly independent of the θ_T cone angle, and thus this barrier decreases from left to right following the inverse trend to the σ-donor ability of the phosphine ligand. In contrast, the relative importance of the tetrahedral cone angle descriptor increases in the transmetalation and reductive elimination barriers. In the case of transmetalation, the barrier increases when moving from small/electron-acceptor ligands such as PF_3 (#20), PCl_3 (#21), PBr_3 (#22) and PI_3 (#23), $PMePh_2$ (#87) or $P(naph)_3$ (#18) among others, to the larger and poorer electron-accepting ligands *i.e.* P*t*Bu_3 (#7), PCy_3 (#10) or PEt_3 (#3). Conversely, the reductive elimination trend barrier increases when going from relatively large and electron-poor ligands ($P(CF_3)_3$ (#24) or $P(C_2F_5)_3$) (#26), to smaller/electron-donating ligands such as PMe_3 (#2), $PHMe_2$ (#67) or PMe_2Et (#74).

4. Conclusions

The Tolman cone angle has been computed, with MM/DFT methodology, for a set of 119 phosphine ligands in three different transition metal coordination environments: linear [AuCl(P)] (θ_L), tetrahedral [$Ni(CO)_3(P)$] (θ_T) and octahedral [$IrCl_3(CO)_2(P)$] (θ_O). As should be expected, the cone angle value decreases when the steric congestion around the metal center increases *i.e.* in general, $\theta_L > \theta_T > \theta_O$.

None of the computed cone angles shows a good linear correlation with the original Tolman cone angle (θ). This is probably due to the flawed formulation of θ, which imposes a compact packing of the ligand substituents and thus produces much lower values than those obtained with the computational approach.

The computed cone angles do not show significant correlations with other steric measures such as the solid angles (Θ), the LKB steric descriptor He_8, or the angular symmetric deformation coordinate (S_4'). In contrast, the computed cone angles show a relatively good correlation with the corresponding percent buried volumes ($\%V_{bur}$), which can be obtained from the most stable computed geometries.

Finally, the computed cone angles can be employed for constructing linear relationships with experimental and computed properties in systems where the phosphine ligand plays a significant role. For instance, the phosphine dissociation enthalpies from open titanocene [Ti(2,4-$C_7H_{11})_2(PR_3)$] complexes can be directly correlated with the octahedral cone angle (θ_O). Finally, the computed tetrahedral θ_T parameter can be used, along with other electronic descriptors, to model the computed reaction barriers for the Suzuki-Miyaura reaction between a monoligated [Pd-PR_3] species and bromobenzene.

5. Supporting Information

Electronic Supplementary Information (ESI) available: schematic representations of biaryl ligands; computed θ_L values for biaryl ligands in their open and close conformations; list of steric descriptors: solid angle (Θ), LKB-P He_8, angular symmetric deformation coordinate (S_4'), and computed $\%V_{bur}$ parameters; computed and predicted ligand dissociation enthalpies from open titanocenes; computed and predicted reaction barriers, and ligand descriptors for the Suzuki-Miyaura reaction between bromobenzene and [Pd-PR_3] catalyst; correlation between θ_T and θ_O with $\%V_{Bur}$ parameters; Force Field parameters used in the MM conformational searches. See DOI: 10.1039/x0xx00000x

6. Author information

jordi.cirera@qi.ub.es

jesus.jover@qi.ub.es

Notes: The authors declare no competing financial interest.

7. Conflicts of interest

There are no conflicts to declare.

8. Acknowledgements

We thank the Spanish Ministerio de Economía y Competitividad for the PGC2018-093863-B-C21 MINECO/FEDER, UE, and Maria de Maeztu (MDM-2017-0767) grants. We are also thankful to S. G. and L. M. for fruitful discussion during the preparation of this manuscript.

9. References

1. A. Cahours and H. Gal, *Justus Liebigs Ann. Chem.*, 1870, **155**, 223-230.
2. J. F. Hartwig, *Organotransition Metal Chemistry: from Bonding to Catalysis*, University Science Books, New York, 2010.
3. J. A. Osborn, F. H. Jardine, J. F. Young and G. Wilkinson, *J. Chem. Soc. A*, 1966, 1711-1732.
4. S. T. Nguyen, L. K. Johnson, R. H. Grubbs and J. W. Ziller, *J. Am. Chem. Soc.*, 1992, **114**, 3974-3975.
5. (a) R. F. Heck, in *Organic Reactions*, 1982, vol. 27, pp. 345-390; (b) A. O. King, N. Okukado and E. I. Negishi, *J. Chem. Soc., Chem. Commun.*, 1977, 683-684; (c) N. Miyaura and A. Suzuki, *Chem. Rev.*, 1995, **95**, 2457-2483; (d) K. Sonogashira, *J. Organomet. Chem.*, 2002, **653**, 46-49; (e) J. K. Stille, *Angew. Chem. Int. Ed.*, 1986, **25**, 508-523.
6. A. Grabulosa, *P-Sterogenic Ligands in Enantioselective Catalysis*, The Royal Society of Chemistry, Cambridge, 2011.
7. C. A. Tolman, 1970, **92**, 2956-2959.
8. (a) C. A. Tolman, *J. Am. Chem. Soc.*, 1970, **92**, 2956-2965; (b) C. A. Tolman, W. C. Seidel and L. W. Gosser, *J. Am. Chem. Soc.*, 1974, **96**, 53-60; (c) C. A. Tolman, *Chem. Rev.*, 1977, **77**, 313-348.
9. (a) J. M. Smith and N. J. Coville, *Organometallics*, 2001, **20**, 1210-1215; (b) K. A. Bunten, L. Chen, A. L. Fernandez and A. J. Poë, *Coord. Chem. Rev.*, 2002, **233-234**, 41-51; (c) R. B. DeVasher, J. M. Spruell, D. A. Dixon, G. A. Broker, S. T. Griffin, R. D. Rogers and K. H. Shaughnessy, *Organometallics*, 2005, **24**, 962-971; (d) L. L. Hill, L. R. Moore, R. Huang, R. Craciun, A. J. Vincent, D. A.

Dixon, J. Chou, C. J. Woltermann and K. H. Shaughnessy, *J. Org. Chem.*, 2006, **71**, 5117-5125; (e) L. L. Hill, J. M. Smith, W. S. Brown, L. R. Moore, P. Guevera, E. S. Pair, J. Porter, J. Chou, C. J. Wolterman, R. Craciun, D. A. Dixon and K. H. Shaughnessy, *Tetrahedron*, 2008, **64**, 6920-6934; (f) L. R. Moore, E. C. Western, R. Craciun, J. M. Spruell, D. A. Dixon, K. P. O'Halloran and K. H. Shaughnessy, *Organometallics*, 2008, **27**, 576-593.

10. (a) N. Fey, A. G. Orpen and J. N. Harvey, *Coord. Chem. Rev.*, 2009, **253**, 704-722; (b) N. Fey, *Dalton Trans.*, 2010, **39**, 296-310; (c) J. A. Bilbrey and W. D. Allen, in *Annual*

Reports in Computational Chemistry, ed. R. A. Wheeler, Elsevier, 2013, vol. 9, pp. 3-23; (d) D. J. Durand and N. Fey, *Chem. Rev.*, 2019, **119**, 6561-6594.

11. (a) A. Immirzi and A. Musco, *Inorg. Chim. Acta*, 1977, **25**, L41-L42; (b) T. L. Brown and K. J. Lee, *Coord. Chem. Rev.*, 1993, **128**, 89-116; (c) D. White, B. C. Taverner, P. G. L. Leach and N. J. Coville, *J. Comp. Chem.*, 1993, **14**, 1042-1049.
12. (a) N. Fey, A. C. Tsipis, S. E. Harris, J. N. Harvey, A. G. Orpen and R. A. Mansson, *Chem. Eur. J.*, 2006, **12**, 291-302; (b) J. Jover, N. Fey, J. N. Harvey, G. C. Lloyd-Jones, A. G. Orpen, G. J. J. Owen-Smith, P. Murray, D. R. J. Hose, R. Osborne and M. Purdie, *Organometallics*, 2010, **29**, 6245-6258; (c) J. Jover, N. Fey, J. N. Harvey, G. C. Lloyd-Jones, A. G. Orpen, G. J. J. Owen-Smith, P. Murray, D. R. J. Hose, R. Osborne and M. Purdie, *Organometallics*, 2012, **31**, 5302-5306; (d) J. Jover and N. Fey, *Dalton Trans.*, 2013, **42**, 172-181.
13. (a) B. J. Dunne, R. B. Morris and A. G. Orpen, *J. Chem. Soc. Dalton Trans.*, 1991, 653-661; (b) K. D. Cooney, T. R. Cundari, N. W. Hoffman, K. A. Pittard, M. D. Temple and Y. Zhao, *J. Am. Chem. Soc.*, 2003, **125**, 4318-4324.
14. (a) A. C. Hillier, W. J. Sommer, B. S. Yong, J. L. Petersen, L. Cavallo and S. P. Nolan, *Organometallics*, 2003, **22**, 4322-4326; (b) H. Clavier and S. P. Nolan, *Chem. Commun.*, 2010, **46**, 841-861.
15. A. Verloop, W. Hoogenstraten and A. Tipker, in *Drug Design*, ed. A. J. Ariens, Academic Press, New York, 1976, vol. II, pp. 165-207.
16. (a) W. Draber, *Naturforsch. C: J. Biosci.*, 1996, **51**, 1-7; (b) K. C. Harper, S. C. Vilardi and M. S. Sigman, *J. Am. Chem. Soc.*, 2013, **135**, 2482-2485; (c) A. H. Christian, Z. L. Niemeyer, M. S. Sigman and F. D. Toste, *ACS Catal.*, 2017, **7**, 3973-3978; (d) R. Ardkhean, M. Mortimore, R. S. Paton and S. P. Fletcher, *Chem. Sci.*, 2018, **9**, 2628-2632.
17. Y. Guan, V. M. Ingman, B. J. Rooks and S. E. Wheeler, *J. Chem. Theory Comput.*, 2018, **14**, 5249-5261.
18. (a) *Molecular Structure Laboratory, Resources, University of Wisconsin. http://xray.chem.wisc.edu/Resources.html (accessed Aug 20, 2019)*; (b) I. A. Guzei and M. Wendt, *Dalton Trans.*, 2006, 3991-3999; (c) Z. L. Niemeyer, A. Milo, D. P. Hickey and M. S. Sigman, *Nat. Chem.*, 2016, **8**, 610.
19. D. Coll, R. Añez, A. Sierraalta, J. Antonio Rodriguez, A. Vidal and E. Ocando, *Inorg. Chim. Acta*, 2015, **436**, 163-168.
20. K. Wu and A. G. Doyle, *Nat. Chem.*, 2017, **9**, 779.
21. J. A. Bilbrey, A. H. Kazez, J. Locklin and W. D. Allen, *J. Comp. Chem.*, 2013, **34**, 1189-1197.
22. Mathematica, version 9.0, Wolfram Research, Inc.: Champaign, Illinois, 2010.
23. J. A. Bilbrey, A. H. Kazez, J. Locklin and W. D. Allen, *J. Chem. Theor. Comp.*, 2013, **9**, 5734-5744.

24. (a) D. W. Old, J. P. Wolfe and S. L. Buchwald, *J. Am. Chem. Soc.*, 1998, **120**, 9722-9723; (b) D. S. Surry and S. L. Buchwald, *Angew. Chem. Int. Ed.*, 2008, **47**, 6338-6361; (c) D. S. Surry and S. L. Buchwald, *Chem. Sci.*, 2011, **2**, 27-50.
25. I. T. Todorov, W. Smith, K. Trachenko and M. T. Dove, *J. Mater. chem.*, 2006, **16**, 1911-1918.
26. J.-D. Chai and M. Head-Gordon, *Phys. Chem. Chem. Phys.*, 2008, **10**, 6615-6620.
27. M. J. Frisch, G. W. Trucks, H. B. Schlegel, G. E. Scuseria, M. A. Robb, J. R. Cheeseman, G. Scalmani, V. Barone, B. Mennucci, G. A. Petersson, H. Nakatsuji, M. Caricato, X. Li, H. P. Hratchian, A. F. Izmaylov, J. Bloino, G. Zheng, J. L. Sonnenberg, M. Hada, M. Ehara, K. Toyota, R. Fukuda, J. Hasegawa, M. Ishida, T. Nakajima, Y. Honda, O. Kitao, H. Nakai, T. Vreven, J. Montgomery, J. A., J. E. Peralta, F. Ogliaro, M. Bearpark, J. J. Heyd, E. Brothers, K. N. Kudin, V. N. Staroverov, R. Kobayashi, J. Normand, K. Raghavachari, A. Rendell, J. C. Burant, S. S. Iyengar, J. Tomasi, M. Cossi, N. Rega, N. J. Millam, M. Klene, J. E. Knox, J. B. Cross, V. Bakken, C. Adamo, J. Jaramillo, R. Gomperts, R. E. Stratmann, O. Yazyev, A. J. Austin, R. Cammi, C. Pomelli, J. W. Ochterski, R. L. Martin, K. Morokuma, V. G. Zakrzewski, G. A. Voth, P. Salvador, J. J. Dannenberg, S. Dapprich, A. D. Daniels, Ö. Farkas, J. B. Foresman, J. V. Ortiz, J. Cioslowski and D. J. Fox Gaussian09, Revision D.01, Gaussian, Inc.: Wallingford CT, 2009.
28. (a) A. Schäfer, H. Horn and R. Ahlrichs, *J. Chem. Phys.*, 1992, **97**, 2571-2577; (b) A. Schäfer, C. Huber and R. Ahlrichs, *J. Chem. Phys.*, 1994, **100**, 5829-5835.
29. (a) A. Bergner, M. Dolg, W. Küchle, H. Stoll and H. Preuss, *Mol. Phys.*, 1993, **80**, 1431-1441; (b) T. H. Dunning and P. J. Hay, in *Modern Theoretical Chemistry*, ed. H. F. Schaefer III, Plenum, New York, 1976, vol. 3, pp. 1-28.
30. S. Grimme, J. Antony, S. Ehrlich and H. Krieg, *J. Chem. Phys.*, 2010, **132**, 154104.
31. (a) C. Lee, W. Yang and R. G. Parr, *Phys. Rev. B*, 1988, **37**, 785-789; (b) B. Miehlich, A. Savin, H. Stoll and H. Preuss, *Chem. Phys. Lett.*, 1989, **157**, 200-206; (c) A. D. Becke, *J. Chem. Phys.*, 1993, **98**, 5648-5652.
32. (a) J. P. Perdew, *Phys. Rev. B*, 1986, **33**, 8822-8824; (b) A. D. Becke, *Phys. Rev. A*, 1988, **38**, 3098-3100.
33. (a) J. P. Perdew, K. Burke and M. Ernzerhof, *Phys. Rev. Lett.*, 1996, **77**, 3865-3868; (b) J. P. Perdew, K. Burke and M. Ernzerhof, *Phys. Rev. Lett.*, 1997, **78**, 1396.
34. C. Adamo and V. Barone, *J. Chem. Phys*, 1999, **110**, 6158-6169.
35. Y. Zhao and D. G. Truhlar, *Theor. Chem. Acc.*, 2008, **120**, 215-241.
36. (a) J. P. Perdew, in *Electronic Structure of Solids '91*, eds. P. Ziesche and H. Eschrig, Akademie Verlag, Berlin, 1991, vol. 11; (b) J. P. Perdew, J. A. Chevary, S. H. Vosko, K. A. Jackson, M. R. Pederson, D. J. Singh and C. Fiolhais, *Phys. Rev. B*, 1992, **46**, 6671-6687; (c) J. P. Perdew, J. A. Chevary, S. H. Vosko, K. A. Jackson, M. R. Pederson, D. J. Singh and C. Fiolhais, *Phys. Rev. B*, 1993, **48**, 4978; (d) J. P. Perdew, K. Burke and Y. Wang, *Phys. Rev. B*, 1996, **54**, 16533-16539; (e) K. Burke, J. P. Perdew and Y. Wang, in *Electronic Density Functional Theory: Recent Progress and New Directions*, eds. J. F. Dobson, G. Vignale and M. P. Das, Plenum, 1998.
37. (a) V. N. Staroverov, G. E. Scuseria, J. Tao and J. P. Perdew, *J. Chem. Phys.*, 2003, **119**, 12129-12137; (b) J. Tao, J. P. Perdew, V. N. Staroverov and G. E. Scuseria, *Phys. Rev. Lett.*, 2003, **91**, 146401.
38. (a) A. D. Becke, *J. Chem. Phys.*, 1997, **107**, 8554-8560; (b) H. L. Schmider and A. D. Becke, *J. Chem. Phys.*, 1998, **108**, 9624-9631; (c) S. Grimme, *J. Comp. Chem.*, 2006, **27**, 1787-1799.

39. S. Grimme, S. Ehrlich and L. Goerigk, *J. Comp. Chem.*, 2011, **32**, 1456-1465.
40. Y. Minenkov, A. Singstad, G. Occhipinti and V. R. Jensen, *Dalton Trans.*, 2012, **41**, 5526-5541.
41. A. Bondi, *J. Phys. Chem.*, 1964, **68**, 441-451.
42. (a) A. Poater, B. Cosenza, A. Correa, S. Giudice, F. Ragone, V. Scarano and L. Cavallo, *Eur. J. Inorg. Chem.*, 2009, **2009**, 1759-1766; (b) L. Falivene, R. Credendino, A. Poater, A. Petta, L. Serra, R. Oliva, V. Scarano and L. Cavallo, *Organometallics*, 2016, **35**, 2286-2293.
43. L. Stahl and R. D. Ernst, *J. Am. Chem. Soc.*, 1987, **109**, 5673-5680.
44. J. Jover, N. Fey, M. Purdie, G. C. Lloyd-Jones and J. N. Harvey, *J. Mol. Catal. A*, 2010, **324**, 39-47.
45. J.-P. Corbet and G. Mignani, *Chem. Rev.*, 2006, **106**, 2651-2710.
46. G. Mann, Q. Shelby, A. H. Roy and J. F. Hartwig, *Organometallics*, 2003, **22**, 2775-2789.